Enhancement of Optical Absorption and Bandgap Decrease of PVDF/Curcuma Longa Linn Composites: UV-Vis Technique

E.A. Falcão*, T. S. Silva, E.S.S. Rodrigues and S.M. Martelli

Post-Graduation Program in Environmental Science and Technology (PPGCTA), Federal University of Grande Dourados (UFGD), Rodovia Dourados-Itahum, km 12, Dourados, MS, Zip: 79.804-970, Brazil

Abstract: In the present work, the polyvinylidene fluoride (PVDF) and PVDF/Curcuma longa Linn (PVDF/CLL) were prepared in five different concentrations. The FT-IR technique was used to analyze the incorporation of CLL in the PVDF matrix. The CLL introduction in the PVDF matrix increases de relative percentage of β phase. The optical properties of PVDF/CLL were studied using UV-Vis spectroscopy. The incorporation of CLL into the PVDF matrix changes the optical absorption in the UV-Vis region and shifts the optical absorption edge to higher wavelengths. The optical transmittance of pure PVDF exceeds 70% from 270 nm to 1400 nm. The addition of 5% CLL reduces optical transmittance by 50%, and at concentrations above 20%, the reduction approaches 100%. The extinction coefficient of PVDF/CLL 10% presents two peaks, one at 234 nm and the other at 421 nm. However, higher concentrations of CLL change the first peak from 234 nm to 247 nm. The skin depth decreases with increasing photon energy. The CLL addition in the PVDF matrix shifts the indirect and direct optical bandgaps towards lower energies. The observed decrease in the bandgap is consistent with the optical absorption edge results. Finally, these results show that PVDF/CLL composites are potential candidates for optical and photonic applications.

Keywords: PVDF, Curcuma longa Linn, Optical bandgap, Ferroelectric polymer, Curcumin.

1. INTRODUCTION

In the last decades, the scientific community has increased its interest in natural materials with multifunctional behavior for different types of applications. Vegetable, pigments and phenolic compounds have been widely studied as sustainable alternatives to conventional additives, especially for their combination of biocompatibility, chemical stability, and lower environmental impact. Among these materials, the curcuma (Curcuma longa Linn), popularly known as turmeric or Indian saffron, belonging to the Zingiberaceae family, is noted as a rich source of bioactive compounds, such as curcuminoids, with curcumin being the most studied component [1]. Curcumin is a polyphenolic pigment with a yellow-orange color, with antioxidant, anti-inflammatory, and antimicrobial activity [1, 2]. Due to its thermal stability, optical properties and conjugated structure by a system π–π*, some studies have highlighted curcumin as an efficient photosensitizer for Dye-Sensitized Solar Cells (DSSCs). These conjugated structures promote electron injection into the conduction band of TiO2, thereby inducing charge recombination and increasing the system's quantum efficiency [3]. Curcumin provides a firm anchorage on semiconductor and polymeric surfaces, thereby improving electronic stability and photoelectric performance [4-5]. Among the polymeric matrices used in solar cells, polyvinylidene fluoride (PVDF) has emerged as one of the best materials for backsheet applications in modern solar panels. Because of its weather and chemical resistance, mechanical strength, temperature, low surface energy, and exceptional dielectric properties [6]. PVDF is a semi-crystalline ferroelectric polymer, which presents five crystalline phases, being the most studied phases α' and β, because of its elasticity, processability, and ferroelectric response [7-10]. PVDF matrix is easily processable and can be prepared with different fillers to enhance its physical properties, such as electrical, dielectric, and optical properties [11-13]. Making this polymeric matrix suitable for optoelectronic applications such as solar cells, light-emitting diodes, optical switches, optical waveguides, nonlinear optical devices, photonic devices, and others [14]. As previously described, both Curcuma longa and PVDF have been studied for optical and photonic applications. Therefore, the objective of this work was to synthesize and characterize the optical properties of PVDF samples doped with curcuma (CLL) or PVDF/CLL at five different concentrations (m/m) via the UV-Vis technique. This technique is a powerful tool for studying the optical properties of many materials. Providing results of optical transmittance, optical absorption coefficient, skin depth, extinction coefficient and optical bandgap.

MATERIALS AND METHODS

PVDF powder used in this work was donated by Arkema of Brazil (Kynar™) without any purification. Vetec™ DMF (99.8% purity) was used as the solvent. Curcuma L. Linn was purchased at a local market. To

*Address correspondence to this author at the Federal University of Grande Dourados (UFGD), Rodovia Dourados-Itahum, km 12, Dourados, ZIP code 79.804-970, MS, Brazil;
E-mail: evaristofalcao@ufgd.edu.br

Received on 00-00-2025 Accepted on 00-00-2025 Published on 00-00-2025

E-ISSN: 2311-8717/25

prepare the filler, CLL roots were washed in a water flow, peeled, sliced, and dried in an oven for 48 h at 50 °C. After this procedure, the material was ground using a knife mill Britania™ BMX400P. The powder particles were sieved through a common sieve purchased at a regular supermarket with an opening of 0.71 mm (25 mesh) to control the size of particles. In brief, to prepare pure PVDF samples, 120 mg of PVDF powder was dissolved in DMF at room temperature. For the PVDF/CLL composites, the CLL loadings were 5%, 10%, 20%, and 30% by mass relative to PVDF. Both PVDF and CLL were dissolved separately in DMF at room temperature to prepare stock solutions. Then, the dissolved PVDF and CLL solutions were mixed, stirred, and placed in glass Petri dishes in their relative proportions. Subsequently, the samples were dried in an oven at 50 °C for 16 h to remove the solvent and form the films. A UV-Vis spectrophotometer, Shimadzu model UV-2700i with Diffuse Reflectance, in the wavelength range of 200–1400 nm, was used to perform UV–Vis measurements, and the LabSolutions acquisition program provided diffuse transmittance and absorbance results. FT-IR/ATR analysis was performed using a Bruker Invenio R spectrometer, equipped with a diamond ATR unit. The scan was performed over 4000-100 cm^{-1} with 64 scans at a resolution of 1 cm^{-1}. Background spectra were automatically recorded and subtracted, and the resulting spectra were saved in OPUS software.

RESULTS AND DISCUSSIONS

The obtained samples had thicknesses of 0,007 ± 0,002 mm, 0,009 ± 0,002 mm, 0,05 ± 0,004 mm, 0,070± 0,001 mm, and 0,048 ± 0,001 mm for PVDF, PVDF/CLL 5%, PVDF/CLL 10%, PVDF/CLL 20%, and PVDF/CLL 30%, respectively. These results are the average of measurements taken at six points on the sample.

In Figure **1**, the FT-IR spectra for pure PVDF and PVDF/CLL composites are represented. Pure PVDF samples exhibit the characteristic absorption peaks of the α' phase at 530, 615, 761, 795, 855, 976, and 1402 cm^{-1} [15]. The β-phase is characterized by peaks at 511, 840 and 1275−1279 cm^{-1}, and the γ phase is characterized by peaks at 778, 812 and 834 cm^{-1} [15]. Pure PVDF also exhibits a characteristic peak between 1242 cm^{-1} and 1064 cm^{-1} due to C–F stretching [15]. The FTIR spectrum of the CLL sample showed characteristic vibrational features consistent with the known spectral profile of curcumin. The band at approximately 1627 cm^{-1} corresponds to the conjugated C=O/C=C stretching of the β-diketone system, a structural signature of the stabilized enolic form of curcumin [16]. In the 1500–1600 cm^{-1} region, the spectrum exhibits the C=C stretching modes of the phenyl rings, arising from internal deformations of the aromatic conjugated system [16]. The band near 1270 cm^{-1} is assigned to C–O/C–OH vibrations of the enol–phenolic group, associated with coupled deformations of the keto–enol system [16, 17]. The band around 1150 cm^{-1} corresponds to C–O–C stretching, a mode characteristic of phenolic and conjugated ether groups commonly found in curcumin and its natural analogues [16, 17]. The signal near 1000 cm^{-1} reflects a combination of C–O stretching and aromatic C–H bending, a mixed vibrational behavior also observed for turmeric extracts cultivated in Yemen and confirmed by FTIR analyses of curcuminoid-containing plant materials [17, 18]. At lower wavenumbers, the band at approximately 850 cm^{-1} corresponds to out-of-plane (C–H) deformation, a typical marker of substituted aromatic rings in curcuminoids [16, 17]. The presence of these features collectively demonstrates that the sample's molecular structure matches the expected vibrational fingerprint of curcumin and related natural derivatives. In this study, the α' peak appears at 761 cm^{-1} for PVDF/CLL 5%. However, for PVDF/CLL 10 %, 20% and 30% α peak is displaced to 769 cm^{-1}, indicating a clear de interaction between PVDF and CLL. It is observed too, that the peak at 871 cm^{-1}, due to the amorphous phase is also displaced. On the other hand, the peak β phase remains unchanged for high concentrations. The observed peak at 1000 cm^{-1}, due to curcumin, is observed in all PVDF/CLL samples, confirming the interaction between CLL and the PVDF matrix.

From the FT-IR absorbance results and using the Salimi-Yousef equation (Eq. 1),

$$F(\beta) = \frac{Abs_{\beta}}{1.26(Abs_{\alpha}+Abs_{\beta})} \quad \text{Eq. 1}$$

it is possible to obtain the relative percentage of β phase [19]. In Eq. 1, A_{α} and A_{β} are the areas of the FT-IR absorption bands at 766 cm^{-1} and 840 cm^{-1}, respectively [19, 20]. The results of the relative percentage of β phase are displayed in Figure **1b**. The CLL addition increases the relative percentage of β phase up to 10 % of CLL addition, and after decreases for PVDF/CLL 20% and 30%. This behavior shows that the CLL addition alters the crystalline phase of the PVDF matrix. However, to understand the phenomenology of the interaction between PVDF and CLL, it is necessary to consider other characterisations.

In Figure **2**, the absorbance and transmittance results are displayed as a function of CLL content. As

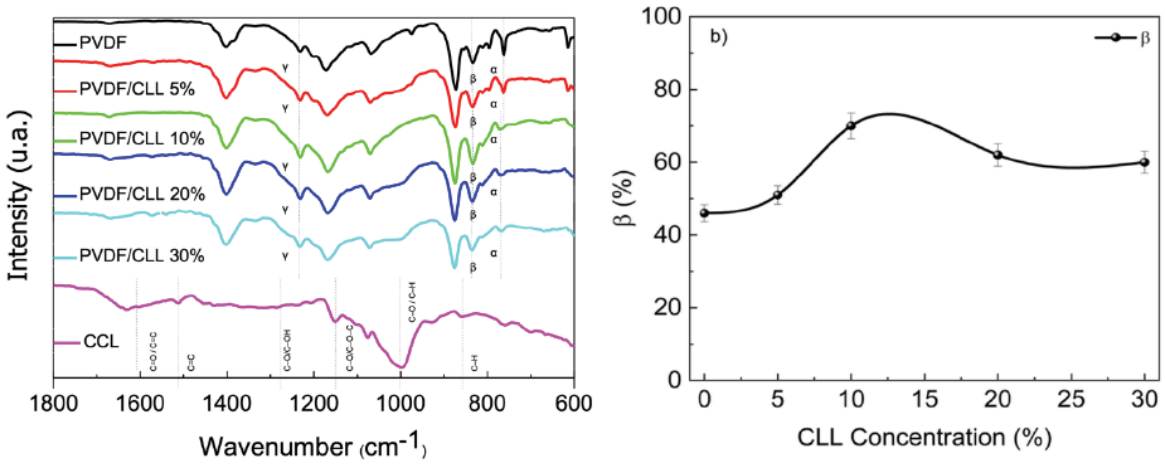

Figure 1: a) FT-IR spectra of PVDF and PVDF/CLL composites as a function of CLL content, and **b**) Relative percentage of β phase as a function of CLL concentration.

shown in Figure **2**(**a**), pure PVDF exhibits its characteristic optical absorption between 250 nm and 400 nm, attributed to the electronic transition of the fluorocarbons (F-C) [15]. For PVDF/CLL composites, adding filler to the PVDF matrix enhances the optical absorbance in the UV region. This behavior might be associated with increasing CLL and, consequently, an increase in curcumin. Curcumin is a yellow-orange polyphenolic pigment with structure that presents hydroxyl and carbonyl groups conjugated by a system π–π*, which results in a high optical absorption between 420 nm and 530 nm [21]. These electronic conjugations are responsible for the electronic transitions π→π* and n→π*, which are directly associated to its photoactive properties. Literature reports that curcumin presents one peak at 233 nm, due to the p–p* transitions of C=C bonds, and other at 422 nm, which corresponds to n–p* transitions of C=O bonds [22]. In Figure **2**(**b**), pure PVDF presents an optical transmittance of over 70% from 270 nm to 1400 nm. However, for PVDF/CLL 5%, the optical transmittance decreases to 55% in the UV region, and for PVDF/CLL 10%, it decreases to 15%. At high concentration, the optical transmittance in this region decreases close to 100%. This behavior is attributed to the high optical absorption of curcumin and other compounds of CLL.

The optical absorption coefficient was determined using Beer-Lambert's formula, $\alpha = 2.303\left(\frac{A}{d}\right)$, where *A* is the optical absorbance and *d* is the thickness of the sample. In Figure **2**, the optical absorption coefficient of the PVDF samples is shown. As aforementioned, the CLL addition increases optical absorption in the UV region. For the PVDF/CLL 30% composite, the bandwidth at half weight is 268 nm, spanning 200–468 nm, almost the entire UV-Vis region. In Figure **3**, the absorption edge is at 255 nm for pure PVDF. In a previous study, the authors found a value of 247 nm [23]. From Figure **3**, the absorption edge is shifted from 255 nm for pure PVDF to 414 nm for PVDF/CLL 30%. According to Mamand, the redshift of the absorption edge might indicate a reduction in the bandgap energy of PVDF/CLL composites [24].

From optical absorption coefficient it is possible to obtain the extinction coefficient (κ) by the follow equation $\kappa = \frac{\alpha\lambda}{4\pi}$, where λ is the wavelength of the

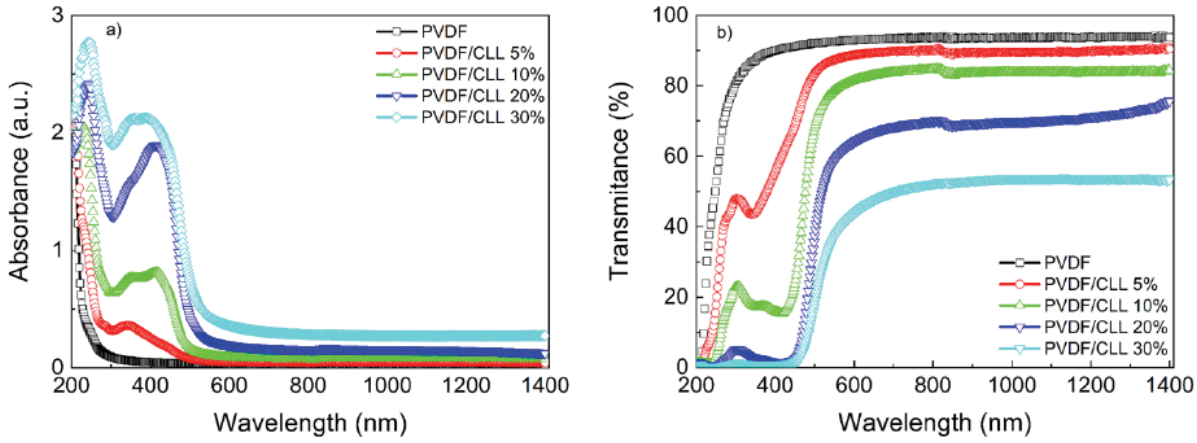

Figure 2: Optical transmittance (**a**) and optical absorbance (**b**) for pure PVDF and doped PVDF/CLL samples.

incident photon. The κ parameter describes the loss of wave energy to the sample, and is the imaginary part of the complex refractive index (ñ) by the following relation (ñ = n + $i\kappa$), where n is the refractive index. Thus, any change observed in the parameter κ directly affects the complex refractive index. In Figure **4a**, the κ values obtained for all PVDF samples are shown. Pure PVDF at 207 nm shows a value of 11.25×10^{-3}, and after κ decreases to 0.48×10^{-3} at 400 nm, then increases. On the other hand, the PVDF/CLL 10 % composite has a value of κ = 1.42 10^{-3} and presents two peaks, one at 234 nm and the other at 421 nm with values of 1.74 x 10^{-3} and $1.24\text{x}10^{-3}$, respectively. For PVDF/CLL 30% at 207 nm, κ = 1.76 × 10^{-3}. However, the first peak of PVDF/CLL 30% increases by $2.61\text{x}10^{-3}$ and shifts from 234 nm to 247 nm, and the second peak increases approximately 164% compared with PVDF/CLL 10%, reaching a value of $3.28\text{x}10^{-3}$ at 421nm. These peaks may be attributed to the curcumin, and the displacement of the first peak from 234 nm to 247 nm might be related to other components of CLL. These results are very important for applications that require UV light absorption, because in this region, the electromagnetic wave loses more energy than at higher wavelengths.

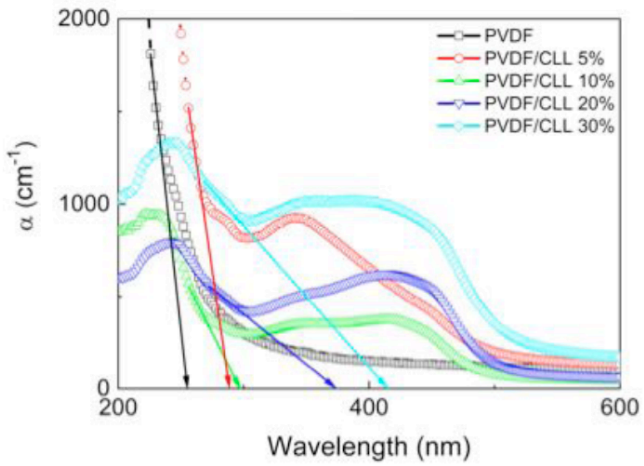

Figure 3: Optical absorption coefficient for PVDF and PVDF/CLL samples as a function of CLL concentration.

It is well known that the optical absorption of electromagnetic waves in semiconductor material depends on many parameters such as thickness, materials type, dopant concentration, photoconductivity, and the extinction coefficient. For the regions of high absorption coefficient for any semiconductor, part of the electromagnetic wave energy is absorbed, leaving only the reflected energy by the material surface [25]. The photon density decreases exponentially from the surface to the middle of the sample, due to material density, surface morphology, refractive index or microstructure [25]. The thickness at which optical photon density becomes 1/e of the value at the surface is called skin depth (δ) or depth penetration [25]. This parameter also depends on the incident photon's conductivity and frequency. Since the conductivity in semiconductors depends on the optical bandgap, it is possible to correlate the optical properties and skin effect in any semiconducting material [25]. Thus, the skin depth is related to the optical absorption coefficient by the following Eq. $\delta = \frac{1}{\alpha}$, where α is the optical absorption coefficient.

In Figure **4b** for pure PVDF at 1 eV, the parameter δ has a value of 0.0112 cm and decreases with increasing incident photon energy, reaching zero at 5.66 eV, the cut-off energy ($E_{cut\text{-}off}$). For the composites at 1 eV, the values obtained were 0.0084 cm, 0.0077 cm, 0.0211 cm, and 0.0285 cm for PVDF/CLL 5%, 10%, 20%, and 30%, respectively, which did not follow a linear trend. This behavior might be associated with surface imperfections or defects induced by the CLL addition. However, further studies are needed to better understand this phenomenon. The results show that δ decreases with increasing photon energy for PVDF and PVDF/CLL composites. For samples with high concentrations of CLL, the $E_{cut\text{-}off}$ is shifted to lower energies. The literature reports that at lower energies, the absorption effect vanishes, the observed reduction occurs over a large distance, and the skin depth increases, indicating an optical transmittance

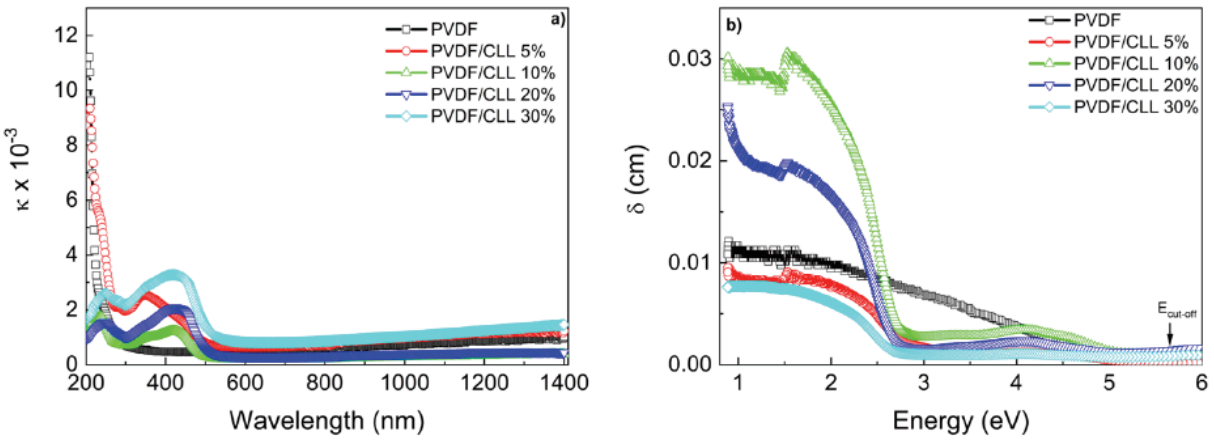

Figure 4: Measurements of Extinction coefficient (**a**) and skin depth (**b**) for pure PVDF and PVDF/CLL samples as a function of CLL concentration.

dependence. Thus, skin depth shows that the CLL addition causes PVDF to lose transparency.

From UV-Vis measurements, the optical bandgap can be estimated. The most common form to calculate the bandgap energy is by the use of Tauc's plot [26]. The frequency-dependent absorption coefficient is given by

$$\alpha h\nu = A\left(h\nu - E_g\right)^r \quad \text{Eq. 1}$$

where *r* is a power factor of the transition mode, E_g is the optical energy gap, and *A* is an energy-independent constant known as the band tailing parameter. Power factor can assume different values, such as 1/2, 2, corresponding to allowed direct, allowed indirect, respectively [14]. Plotting $(\alpha h\nu)^{\frac{1}{r}}$ against the photon energy (hv), and by the extrapolation of the linear portion up to this intercept energy axis, it is possible to find E_g values. In this work, the direct and indirect optical bandgaps were calculated to understand the material's electronic properties. An indirect bandgap is important for understanding electrical conductivity and thermodynamic behavior, and a direct bandgap is important for understanding optical transitions, which influence absorption and light-emitting fluorescence [24]. Thus, both bandgap considerations provide more information about the suitability of the studied material for different applications [24]. Figure **5** presents the Tauc plot for PVDF/CLL samples considering an indirect (Figure **5a**) and a direct (Figure **5b**) bandgap. Pure PVDF exhibited indirect and direct bandgap values of 5.1 eV and 5.6 eV, respectively. In a previous work, it was found that pure PVDF has bandgap values of 4.82 and 5.56 for the indirect and direct bandgaps, respectively [14]. Indolia reported values of 4.96 and 5.66 for the indirect and direct bandgaps [27]. Thus, the results obtained in this work are consistent with previous reports in the literature. In Figure **5**, the behavior of indirect and direct bandgap energies is shown. As can be seen both the indirect and direct bandgaps decrease with increasing CLL content. The CLL addition might contribute to states near the band edges, thereby lowering the Fermi level and narrowing the bandgap [27]. Also, the bandgap decrease might be associated with structural changes caused by the filler and show compositional dependence. Another explanation for the decrease in optical energy might be the formation of defects that alter optical properties. A decrease in bandgap also indicates an increase in the electrical conductivity of the PVDF/CLL composites. The optical bandgap behavior is consistent with the previous result for the optical absorption edge.

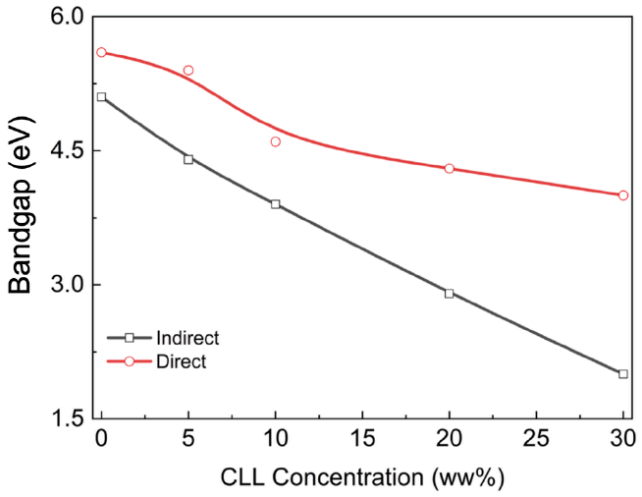

Figure 6: Comparison between indirect and direct energy band gap of PVDF and PVDF/CLL composites.

Ater find bandgap the power factor can be obtained from the slope of the straight-line plot of $ln(\alpha h\nu)\ vs\ ln\left(h\nu - E_g\right)$. The *r* obtained for pure PVDF, PVDF/CLL 5%, PVDF/CLL 10%, PVDF/CLL 20%, and PVDF/CLL 30% were 2.29, 2.19, 2.18, 1.87, and 1.89, respectively. In a previous work, for the indirect bandgap, it was found *r* = 1.92, and in this work *r* ≈ 2 [14]. Thus, the results indicate an indirect bandgap transition and agree with the literature [14, 23].

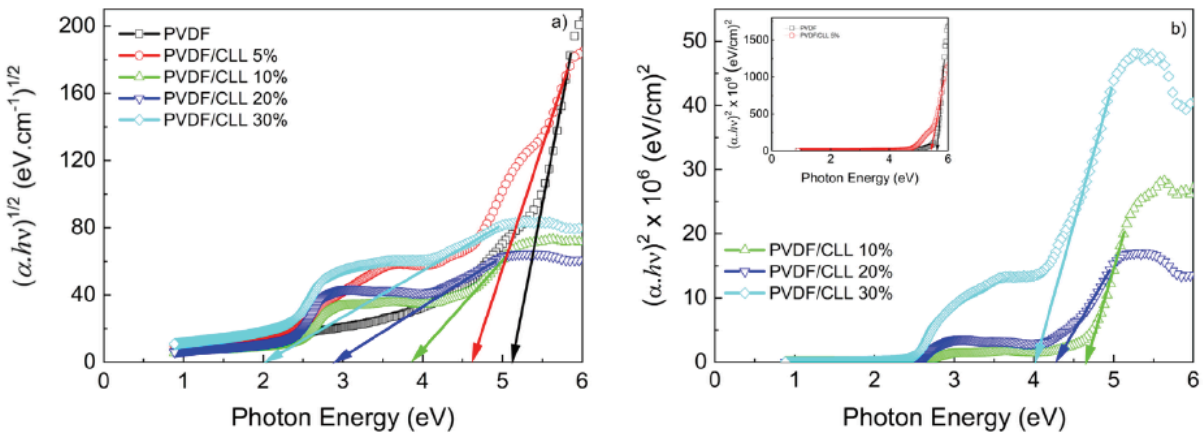

Figure 5: Tauc plot indirect (**a**) and direct (**b**) optical energy bandgap for pure PVDF and PVDF/CLL composites as a function of CLL concentration.

Considering now a direct bandgap, the values found were 0.50, 0.49, 0.50, 0.45, and 0.53 for PVDF, PVDF/CLL 5%, PVDF/CLL 10%, PVDF/CLL 20%, and PVDF/CLL 30%, respectively. Alhassan *et al*. report that semicrystalline polymers, such as PVDF, may exhibit both direct and indirect energy bandgaps [28].

CONCLUSION

In this study, Curcuma longa Linn was used as a filler in the PVDF matrix. FT-IR measurements have been performed to confirm the incorporation of CLL into the PVDF matrix. FT-IR results revealed an increase in the β phase, attributed to the interaction between PVDF and CLL. The UV-Vis technique was successfully applied to analyze changes in the optical properties of the PVDF matrix induced by CLL addition. The addition of CLL to the PVDF enhancemes the optical absorption in the UV-Vis region. This behavior was attributed to the curcumin present in Curcuma longa Linn and confirmed by FT-IR measurements. For pure PVDF, the optical transmittance exceeds 70% from 270 nm to 1400 nm. However, for PVDF/CLL, 20% and 30% optical transmittance are close to 0%. The extinction coefficient for PVDF/CLL 10% shows two peaks, one at 234 and the other at 421, attributed to curcumin. For PVDF/CLL 20% and 30% the first peak is shifted from 234 nm to 247 nm. This displacement might be associated with the other components present in the Curcuma longa Linn. The observed increase of κ at UV-Vis indicates that the light absorption electromagnetic wave in this region loses more energy than higher wavelengths. Skin depth results show that PVDF/CLL composite addition did not present a linear trend with the CLL addition. This behavior might be associated with surface imperfections or defects induced by CLL. The CLL concentration also shifts the $E_{cut\text{-}off}$ toward lower energies, causing PVDF to lose its transparency. The results show that the bandgap energy decreases with increasing CLL content, corroborating the trend observed for the optical absorption edge. The bandgap decrease might be associated with defects or structural disorder, which increases the density of localized states introduced by CLL. However, further studies should be conducted on PVDF/CLL composites to understand the phenomenology underlying these parameters. Finally, the results show that PVDF/CLL composites are promising candidates for optical and photonic applications, as well as for devices requiring UV protection.

AUTORS'CONTRIBUTION

T. S. Silva, Sample preparation, Investigation, **E. S. S. Rodrigues:** Sample preparation, Investigation, **S. M Martelli**: Formal analysis, Conceptualization, Methodology, Review & editing., **E.A. Falcao**: Project administration, Supervision, Conceptualization, Methodology, Resources, Investigation, Visualization, Formal analysis, Writing - original draft, review & editing.

ACKNOWLEDGEMENTS

The authors are grateful to the Brazilian Agencies: CAPES, CNPq (process 483683/2010-8), FINEP (contract 04.13.0448.00/2013), and FUNDECT (process 83/026.883/2024) for the financial support of this work.

DECLARATION OF CONFLICTING INTEREST

The authors of this work declare that there is no conflict of interest in the submission of this manuscript, and it was approved by all authors for publication.

REFERENCES

[1] J. S. Rad, Y. El Rayess, A. A. Rizk, *et al*. Turmeric and its Major Compound Curcumin on Health: Bioactive Effects and Safety Profiles for Food, Pharmaceutical, Biotechnological And Medicinal Applications. Front. in Pharm., v. 11, p. 1021, 2020. https://doi.org/10.3389/fphar.2020.01021

[2] A. M. Shabrina, R. S. S. Azzahra, *et al*. Potential of Natural-Based Sun Protection Factor(SPF): a Systematic Review of Curcumin as Sunscreen. Cosmetics, v. 12, n. 1, p. 10, 2025. https://doi.org/10.3390/cosmetics12010010

[3] J. P. Ayoub, G. T. Tractz, B. V. Dias, E. P. Banzcek, P. R. P. Rodrigues, Comparative Study of Curcuma Longa and Beta Extracted dye Applied on Dye Sensitized Solar Cells. Ver. Virt. de Química, v. 11, n. 6, p. 1908- 1919, 2019. https://doi.org/10.21577/1984-6835.20190133

[4] L. Michels, A. Richter, R. K. Chellappan *et al*., Electronic and Structural Properties of the Natural Dyes Curcumin, Bixin and Indigo. RSC Advances, v. 11, p. 14169- 14177, 2021. https://doi.org/10.1039/D0RA08474C

[5] F. Yuliasari, U. Nuraini, A. R. Aeni, R. Hidayat, Fabrication of Dye-Sensitized Solar Cells With Natural Dye Pigments Derived From Mustard Green (Brassica juncea L.) and Turmeric (Curcuma longa L). Journal of Physics: Conference Series, v. 2866, p. 012013, 2024. https://doi.org/10.1088/1742-6596/2866/1/012013

[6] M. Younas, A. Khan, D. Amjad, M. A. Rehman, A. N. A. Farhad, U. Mehmood, Development of Robust Polyvinylidene Fluoride (PVDF)-based Self-Clean Coating for Commercial Solar Cells/Panels Employing Spray Method, Mat. Lett. 355, 2024, 135486. https://doi.org/10.1016/j.matlet.2023.135486

[7] Ahmed, S.K. Raghuvanshi, N.P. Sharma, J.B.M. Krishna, M.A. Wahab, 1.25mev Gamma Irradiated Induced Physical and Chemical Changes in Poly Vinylidene Fluoride (PVDF) Polymer, Prog. Nanotechnol. Nanomater. 2 (2013) 42-46.

[8] A. Moslehyani, A.F. Ismail, M.H.D. Othman, T. Matsuura, Design and Performance Study of Hybrid Photocatalytic Reactor-PVDF/ MWCNT Nanocomposite Membrane System for Treatment Of Petroleum Refinery Wastewater, Desalination 363 (2015) 99-111. https://doi.org/10.1016/j.desal.2015.01.044

[9] H. Li, W. Chen, Y. Sun, X. Huang, G. Yu, Adsorbing a PVDF Polymer via Noncovalent Interactions to Effectively Tune the Electronic and Magnetic Properties of Zigzag Sic Nanoribbons, Phys. Chem. Chem. Phys. 17 (2015) 24038-24047. https://doi.org/10.1039/C5CP03482E

[10] P. Anithakumari, B.P. Mandal, E. Abdelhamid, R. Naik, A.K. Tyagi, Enhancement of Dielectric, Ferroelectric and Magneto-Dielectric Properties in PVDF- Bafe12o19 Composites: A Step Towards Miniaturizated Electronic Devices, RSC Adv. 6 (2016) 16073- 16080. https://doi.org/10.1039/C5RA27023E

[11] Z. Guo, E. Nilsson, M. Rigdahl, B. Hagström, Melt Spinning of PVDF Fibers with Enhanced β Phase Structure, J. Appl. Polym. Sci. 130 (2013) 2603- 2609. https://doi.org/10.1002/app.39484

[12] A.N. Alias, Z.M. Zabidi, A.M.M. Ali, M.K. Harun, Optical Characterization and Properties of Polymeric Materials for Optoelectronic and Photonic Applications, Int. J. Appl. Sci. Technol. 3 (2013) 11-38

[13] T. K. Sinha, S.K. Ghosh, R. Maiti, S. Jana, B. Adhikari, D. Mandal, S.K. Ray, Graphene-Silver Induced Self-Polarized PVDF Based Flexible Plasmonic Nanogenerator Towards the Realization for New Class of Self Powered Optical Sensor, ACS Appl. Mater. Interfaces 8 (2016) 14986- 14993. https://doi.org/10.1021/acsami.6b01547

[14] E. A. Falcao, L. W. Aguiar, R. Guo, A. S. Bhalla, Optical Absorption of Nd2O3-Doped Polyvinylidene Fluoride Films, Mat. Chem. and Phys. 258 (2021) 123904. https://doi.org/10.1016/j.matchemphys.2020.123904

[15] L. W. Aguiar, E.R. Botero, E. A. Falcao et. al., Study of the Changes in The Polar Phase and Optical Properties of Poly(Vinylidene Fluoride) Matrix By Neodymium Compound Addition, Mat. Tod. Comm. 25 (2020) 101274. https://doi.org/10.1016/j.mtcomm.2020.101274

[16] C. S. Mangolim, C. Moriwaki, A. C. Nogueira, F. Sato, M. L. Baesso, A. N. Medina, G. Matioli, Curcumin- β-cyclodextrin Inclusion Complex: Stability, Solubility, Characterization by FT-IR, FT-Raman, X-Ray Diffraction and Photoacoustic Spectroscopy, And Food Application, Food Chem, l [153] (2014) 361- 370. https://doi.org/10.1016/j.foodchem.2013.12.067

[17] Putri, A. S.; Octavianty, T. D.; Wahyudi, N. T.; Safitri, A., Preparation of nanoparticles from Curcuma longa L. and Cosmos caudatus extracts, J. of Phys.: Conf. Series, S.l., v. 1374, p. 012027, 2019. https://doi.org/10.1088/1742-6596/1374/1/012027

[18] H. S. Gumiah, E. A. L. Shaibani, A. E. Shaibany, A. A. Almalady, B. Y. AL Khateeb, S. H. Alharethi, N. AL-Gabri, A. H. AL Hamsory, F. H. A. L. Futini, Evaluation of Anti-Oxidant and Anti-Cancer Activity of Cultivated Yemeni Curcuma Longa L. Extracts on Skin (A431) and Lung (A549) Cancer Cell Lines. Int. J. of Res. and Develop. in Pharm. & Life Sci., S.l., v. 8, n. 2, 2022

[19] A. Salimi, A.A. Yousef, Analisis method: FTIR Studies of β-phase Crystal Formation in Stretched PVDF Films, Polym. Test. 22 (2003) 699- 704. https://doi.org/10.1016/S0142-9418(03)00003-5

[20] R. Gregorio, M. Cestari, Effect of Crystallization Temperature on the Crystalline Phase Content and Morphology of Poly (vinylidene Fluoride), J. Polym. Sci. Part B: Polym. Phys. 32 (1994) 859- 870. https://doi.org/10.1002/polb.1994.090320509

[21] R. F. Marín, S. C. M. Fernandes b, Mª A. A. Sánchez, J. Labidi, Halochromic And Antioxidant Capacity of Smart Films of Chitosan/Chitin Nanocrystals with Curcuma Oil and Anthocyanins. Food Hydroc., 123 (2022) 107119. https://doi.org/10.1016/j.foodhyd.2021.107119

[22] S. Wilczwiski, K. Skórczewska, J. Tomaszewska, *et al*., Graphene Modification by Curcuminoids as an Effective Method to Improve the Dispersion and Stability of PVDF/Graphene Nanocomposites, Molecules 28 (2023) 3383. https://doi.org/10.3390/molecules28083383

[23] E. A. Falcao, L.W. Aguiar, A.S. Bhalla, *et al*., Ultraviolet Optical Absorption Enhancement and Bandgap Decrease in PVDF Matrix Promoted by the Addition ff Nd/Trans-3,4-(Methylenedioxy) Cinnamic Complex, Mat. Lett. 367 (2024) 136647. https://doi.org/10.1016/j.matlet.2024.136647

[24] D. M. Mamand, D. S. Muhammad, S. B. Aziz, Peshawa O. Hama, B. A. Al-Asbahi, A. A. A. Ahmed, J. Hassan, Enhanced Optical Properties of Chitosan Polymer Doped with Orange Peel Dye Investigated Via UV- Vis and FTIR analysis. Sci Rep15, 3232 (2025). https://doi.org/10.1038/s41598-025-87425-6

[25] A.S. Hassanien, Alaa A. Aki, Effect of Se Addition on Optical and Electrical Properties of Chalcogenide CdSSe Thin Film, Sperl. and Microst. 89 (2016) 153-169. https://doi.org/10.1016/j.spmi.2015.10.044

[26] J. Tauc, R. Grigorovici, A. Vancu, Optical Properties and Electronic Structure of Amorphous Germanium, Phys. Status Solidi 15 (1966) 627-637. https://doi.org/10.1002/pssb.19660150224

[27] A. P. Indolia, M.S. Gaur, Optical Properties of Solution Grown PVDF-ZNO Nanocomposite Thin Films, J. Polym. Res. 20 (2013) 43-51. https://doi.org/10.1007/s10965-012-0043-y

[28] S. Alhassan, K. Alshammari, M. Alshammari, T. Alotaibi, A. H. Alshammari, Y. Fawaz, T.A. Taha, M. Henini, Synthesis and Optical Properties of Polyvinylidene Difluoride Nanocomposites Comprising MoO3/g-C3N4, Resu. in Phys. 48 (2023) 106403. https://doi.org/10.1016/j.rinp.2023.106403

https://doi.org/10.12974/2311-8717.2025.13.09